MISR CMVs and Multiangular Views of Tropical Cyclone Inner-Core Dynamics

Dong L. Wu[1], David J. Diner[1], Michael J Garay[2], Veljko M. Jovanovic[1], Jae N. Lee[1], Catherine M. Moroney[1], Kevin J. Mueller[1], and David L. Nelson[2]

1. Jet Propulsion Laboratory, California Institute of Technology, Pasadena, California

2. Raytheon Intelligence and Information Systems, Pasadena, California

Abstract – Multi-camera stereo imaging of cloud features from the MISR (Multiangle Imaging SpectroRadiometer) instrument on NASA's Terra satellite provides accurate and precise measurements of cloud top heights (CTH) and cloud motion vector (CMV) winds. MISR observes each cloudy scene from nine viewing angles (Nadir, ±26º, ±46º, ±60º, ±70º) with ~400 km swath and 275-m pixel resolution. This paper provides an update on MISR CMV and CTH algorithm improvements, and explores a high-resolution retrieval of tangential winds inside the eyewall of tropical cyclones (TC). The MISR CMV and CTH retrievals from the updated algorithm are significantly improved in terms of spatial coverage and systematic errors. A new product, the 1.1-km cross-track wind, provides high accuracy and precision in measuring convective outflows. Preliminary results obtained from the 1.1-km tangential wind retrieval inside the TC eyewall show that the inner-core rotation is often faster near the eyewall, and this faster rotation appears to be related linearly to cyclone intensity.

Introduction

Cloud and water vapor features have been used to track atmospheric motion vectors (AMVs) from geostationary (GEO) platforms [Nieman et al. 1997; Velden et al., 1997] and from polar-orbiting satellites [Key et al., 2003], with precision on the order of 4-7 m/s [Menzel 2001]. GEO satellites have the advantage of providing continuous coverage of the same location at low and middle latitudes while polar orbiters can provide coverage of high latitudes. GEO sensors with higher temporal sampling, the so-called rapid scan mode, are particularly useful for tropical cyclone (TC) monitoring, but the accuracy of height registration and horizontal resolution of AMVs remain insufficient to provide the needed details for studying TC inner-core dynamics [Velden et al., 2005].

Recently, satellite stereo-photogrammetry has emerged as a viable technique for deriving cloud motion vector (CMV) winds with accurate height assignments [Horváth and Davies, 2001; Zong et al., 2002; Davies et al., 2007]. By acquiring imagery at multiple along-track view angles, the stereo technique overcomes some of the limitations in other AMV methods, and enables simultaneous retrievals of cloud top height (CTH) and cloud motion at a high spatial resolution. The MISR (Multiangle Imaging SpectroRadiometer) instrument on NASA's Terra satellite employs nine viewing angles (Nadir, ±26°, ±46°, ±60°, ±70°) and four spectral bands (446, 558, 672, 866 nm) with a swath of ~400 km and has been in operation since 2000 [Diner et al., 2005]. In particular, the MISR red (672 nm) band channel retains a 275-m pixel resolution at all the viewing angles, and is currently used for global CMV and CTH retrievals.

The MISR instrument has several advantages over other passive techniques for CMV and CTH measurements. First, it does not require knowledge of atmospheric thermal structure, which could lead to large error in height registration at mid-to-high latitudes or in the boundary layer where the temperature lapse rate is small or reversed [e.g., Holz et al., 2008; Garay et al., 2008]. In atmospheric regions with strong vertical wind shear, this error in height registration may induce systematic biases in CMV. Second, MISR 275-m resolution allows CMV and CTH to be retrieved at 1.1 km resolution, which is critical for observing small-scale dynamics and processes such as rotation inside TC eyewalls. Third, MISR data are digitized to 14 bits, which yields a larger dynamic range than 10-bit or 12-bit sensors for extracting feature details in pattern detection and matching.

This paper provides an update on MISR CMV and CTH measurements, and applies the MISR CMV technique to high-resolution observations of TC inner-core dynamics. The MISR CMV and CTH retrievals from the new algorithm have significantly improved spatial coverage and reduced systematic errors compared to the current standard CMV and CTH products. A new product, the 1.1-km cross-track wind, shows very high accuracy and precision in measuring convective outflows at the top of cloud deck. Preliminary results of the 1.1-km tangential wind retrieval inside the TC eyewall show the valuable quality of these high-resolution retrievals, from which we derive tangential wind speeds as a function of radius. We find that the inner-core rotation is often faster near the eyewall, and this faster rotation appears to be related linearly to cyclone intensity. The recent MISR CMV and CTH improvements and high-resolution TC observations are highlighted below.

MISR CMV and CTH

MISR Technique

MISR resolves cloud motion and height within 7 min between the first and last camera. As illustrated in Figure 1, the three near-nadir cameras, each separated by 26° in viewing angle and 46 s in time in sighting the same cloud feature, can measure cloud disparities independently in the along-track (i.e., parallax) and cross-track direction. The parallax, or along-track disparity (displacement), provides a direct measure of CTH in the absence of along-track cloud motion (namely, CMVat) while the cross-track disparity is completely due to the cloud motion in that direction, or CMVct. In the case where CMVat is not zero, the disparity effects from CTH and CMVat are highly correlated and practically indistinguishable if only three near-nadir cameras are used. In order to retrieve both CTH and CMVat simultaneously, one needs to use the parallaxes acquired from more oblique angles where the curvature of Earth's surface helps to break the degeneracy [Zong et al., 2002].
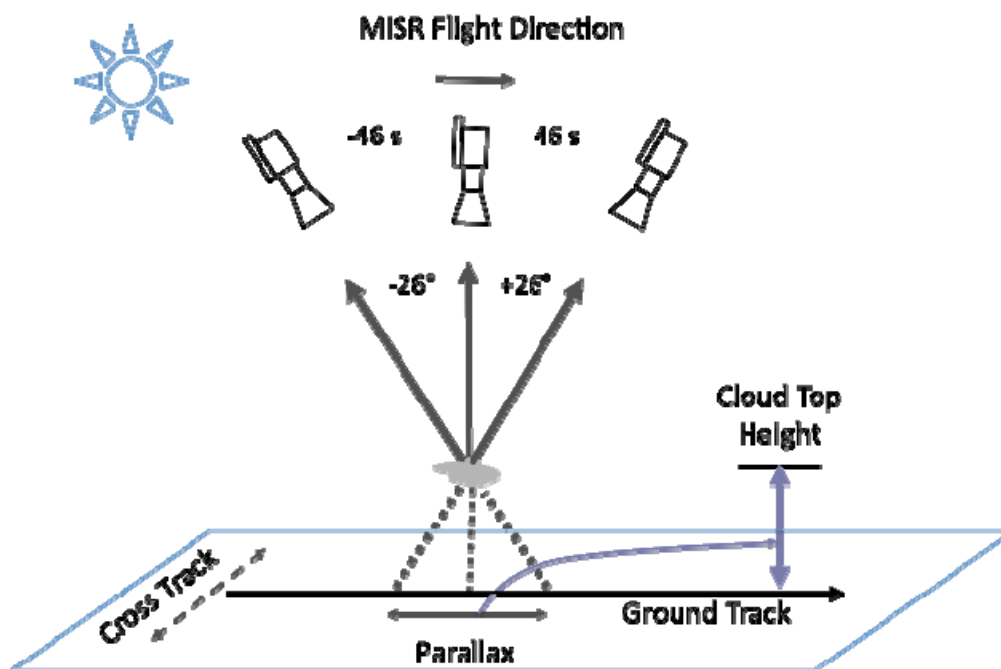

Figure 1. Schematic diagram to show MISR stereo technique in measuring CTH and cross-track CMV (CMVct) from disparities of cloud features in three consecutive views of a MISR flyby. The along-track disparity, or parallax, produces CTH in the absence of along-track CMV (CMVat), whereas the cross-track disparity is independent of parallax and produces the CMV in that direction. In the presence of CMVat, oblique viewing cameras can be used to break the degeneracy between the CMVat and CTH.

Like other CMV techniques, the MISR retrieval seeks to recognize and match feature patterns from their consecutive radiance images of the same scene. Along with its strengths, the cloud pattern matching technique from satellite imagery has certain caveats:

1. Clouds are non-rigid not only because their boundary is not well defined but also their shape may grow/dissipate with time. Thus, the features detected by MISR are required to be relatively stable during the time span of observation in order to produce a valid stereo result. If the retrieval uses the three near-nadir cameras., which spans 92 sec in time, this requirement for stable cloud features can be met in most of the cases since clouds would not grow much in a shorter time period.

2. Multi-layer clouds and vertical wind shears can complicate the pattern matching. MISR near-nadir cameras often catch the most contrast-laden radiance patterns in a specified domain, such as low-level liquid clouds. Tenuous cirrus clouds often appear featureless to MISR. Thus, the standard MISR CTH retrieval is more sensitive to low clouds compared to infrared techniques [Wu et al., 2009]. To observe more high tenuous clouds, one would need to use images from the oblique cameras, from which the forward scattering of clouds is enhanced [Mueller et al., 2008].

3. The spatial scales of cloud and aerosol (e.g., dust and smoke) features vary largely from scene to scene. Thus, performing pattern matching at a finer resolution would better recognize features from different altitudes and produce CMVs with the correct height registration. On the other hand, the accuracy of pattern characterization is governed by the number of pixels used. A fewer number of pixels for pattern matching produces noisier CMVs and is vulnerable to cloud variability. For any given scene, there is an optimal balance between horizontal resolution and CMV quality, Currently, the MISR standard CMV product retrieves CMV at 70.4 km resolution, which is coarser than the optimal resolution for many, if not most, cloudy scenes. The MISR team is evaluating the CMV retrievals at 35.2 km and 17.6 km.

4. Clouds are three-dimensional (3-D) features. Most of the cloud pattern detection/matching techniques are based on 2-D imagery, assuming that the features are flat within a specified horizontal resolution. Such a condition may not be valid in the TC eyewall where the slope is steep, which often result in no retrieval or poor CMV precision.

5. CMVs are not true AMVs in a sense that clouds are not a perfect tracer of atmospheric air. Therefore, interpretation of CMVs requires further investigations. For example, wave clouds from orographic features (i.e., mountains and islands) tend to be stationary even though they are generated by a large background wind; vigorous deep convective clouds in a background flow could yield a slow bias since heavy clouds may not move together with the flow.

MISR Data and Recent Algorithm Improvements

In the MISR standard CMV product, the nadir, 46º and 70º triplet are used for pattern matching and the retrieved CMVs have to pass a quality check between the fore and aft triplets. The method is fast enough to produce CMVs at 70.4 km horizontal and ~500 m vertical resolution, and has been implemented in MISR routine level 2 processing [Moroney et al., 2002]. Several validation studies have been carried on this product, showing that the CMVat precision is generally poorer (3-5 m/s) than the CMVct precision (~1 m/s) [Marchand et al, 2007; Hinkelman et al., 2009], as expected given the need to break the degeneracy between CTH and CMVat.

Figure 2 summaries MISR zonal and meridional CMVs by comparing them with collocated NCEP reanalysis winds for January 2005. Since MISR CMVs are not assimilated in the reanalysis, they provide an independent data source to validate the reanalysis results. As shown for the zonal component, the morphologies of the two data sets are strikingly similar with a consistent distribution in both hemispheres. However, the NCEP zonal winds are generally faster by 8-12 m/s in the Northern Hemisphere (NH) jet. In the Southern Hemisphere (SH) polar region, MISR observations indicate a significant westward motion of ~10 m/s in the upper troposphere (UT) where NCEP winds show a small or opposite flow. For the meridional component, hemispheric differences are obvious, showing smaller biases in the NH. NCEP meridional winds generally lack poleward motion in the cloudy regions at high latitudes. For example, MISR observations indicate a strong poleward motion of 10-20 m/s associated with the clouds in the SH where the winds are much weaker in the NCEP data. Lack of radiosonde data in the SH could explain why the SH reanalysis winds have a larger difference from the observations.
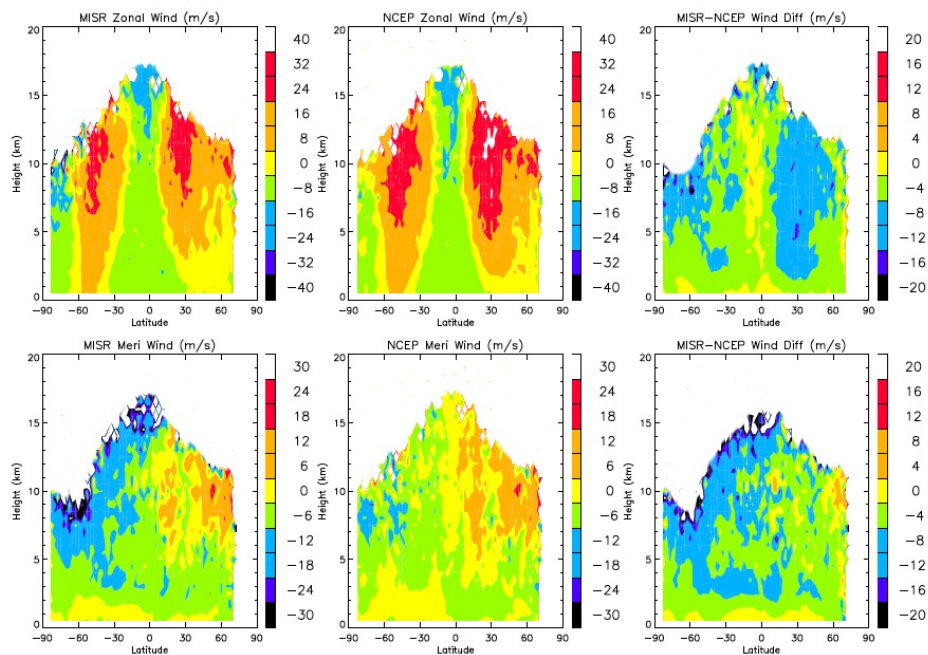

Figure 2. MISR CMV and collocated NCEP zonal (top panel) and meridional (bottom) winds for January 2005. Colors are labeled in m/s, and the differences between MISR and NCEP are shown in the rightmost panels.

The vertical resolution of CMV is critical for studying the atmospheric boundary layer (ABL) where wind speeds are weak and the layers are narrow. In this region, CMV height registration must be sufficiently accurate to characterize the flow, and provides a challenging case for validating MISR and NCEP winds. As shown in Figure 3, convergence at the tropics is stronger and sharper in the MISR meridional CMV than in the reanalysis. The strong convergent flow observed by MISR in the tropics appears to be consistent with the climatology of deep convective cloud bands in the intertropical convection zone (ITCZ).

Encouraged by the successful 70.4-km CMV retrievals, hereafter referred to as the "OLD-70.4 km" method, the MISR team is developing a new version of the CMV retrieval algorithm, namely the "NEW-70.4 km" method, and a corresponding research algorithm at 35.2 km resolution, or the "NEW-35.2 km". The NEW-70.4km algorithm is to be delivered to NASA's data center in the next software delivery cycle and contains significant improvements over the OLD-70.4km retrieval. As shown in

Figure 4 and Figure 5, the NEW-70.4km algorithm provides better coverage of CMV within the MISR swath. This improvement results primarily from enhanced pattern matching and data binning methods. Because of wind variability, retrieval of CMVs at finer resolution is also expected to improve coverage. Preliminary results show that the NEW 35.2-km CMV retrievals significantly improve coverage without degradation of accuracy relative to the NEW 70.4 km retrieval. Both accuracy and coverage of the NEW 35.2-km appear to be superior to the OLD 70.4 km retrieval.

In addition to the coverage improvement, the NEW 70.4-km retrieval fixes known artifacts in the OLD 70.4-km algorithm. Angular histograms of CMV in Figure 5 show that the new algorithm does not suffer from the sampling dropoffs as in the OLD 70.4-km algorithm. The dropoffs in the number of samples appear sharply at the eastward/westward and northward/southward directions in the OLD 70.4-km retrievals, which are not seen in the NCEP or other reanalysis data.
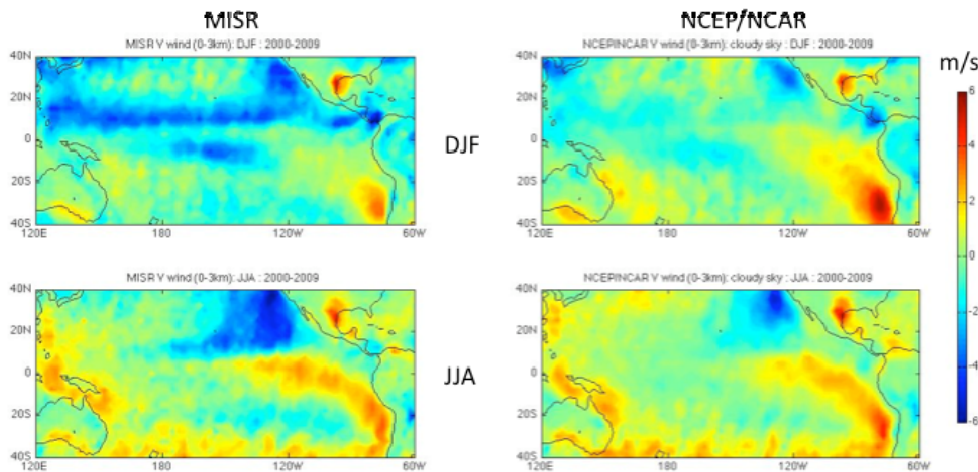

Figure 3. Meridional mean winds (2000-2009) from MISR CMV and collocated NCEP/NCAR reanalysis at heights < 3 km for DJF (top) and JJA (bottom). Convergence of the meridional winds in the Pacific ITCZ is much stronger and sharper in MISR data than in the reanalysis for both DJF and JJA seasons, implying different convection strength and distribution represented by these data sets.

As in the previous MISR standard cloud products, the CTH from the new algorithm is still retrieved at 1.1 km resolution, but with improved performance. As illustrated in

Figure 6, sun-glint contamination and height quantization in the CTH data are greatly reduced. Radiances affected by sun-glint tend to confuse the pattern matcher and create random CTHs. The new algorithm provides a better approach to screening for sun-glint, and as seen in

Figure 6, randomly-distributed CTH from the sun-glint regions are identified and excluded in the output. Another improvement is the reduction of quantization error in the CTH retrieval. The pattern matcher employed in MISR production software outputs pattern disparities at pixel-resolution (275 m) due to the computational constraints. Given advances in computer speed, the new algorithm can afford of a sub-pixel matching. As a result, quantization error is significantly reduced. This improved CTH quality is critical for boundary process studies because of the relatively shallow ABL.
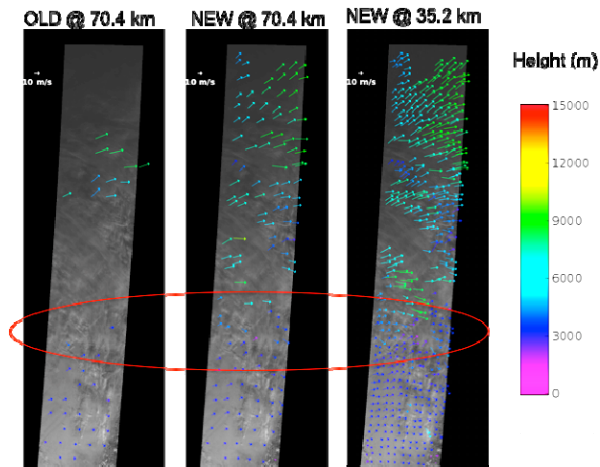

Figure 4. Improvements of the NEW over OLD MISR CMV retrievals. The NEW 70.4-km and 35.3-km algorithms provide a better coverage than the OLD 70.4-km algorithm within the MISR swath. As highlighted by the cycle, the 35.2-km algorithm provides more coverage than the NEW 70.4-km algorithm. The scene is over the Tibetan Plateau and MISR CMVs are colored according to their height assignment.
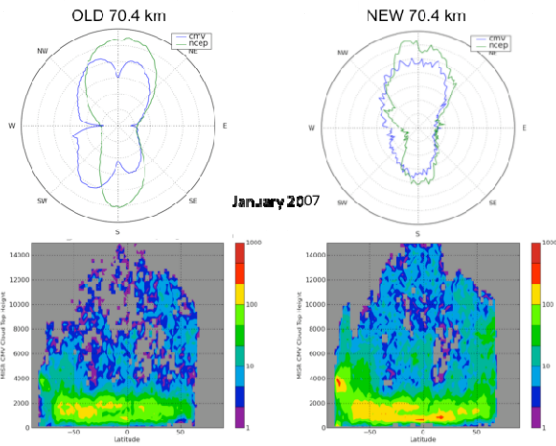
Figure 5. Improvements of the NEW 70.4-km over OLD 70.4-km retrievals in:

Upper panel: Reduction of the sampling dropoff at the eastward/westward and northward/southward directions;

Lower panel: Sampling coverage in latitude-altitude distribution. The data from January 2007 are used for the statistics and color bars denote the number of samples at each latitude-altitude bin.
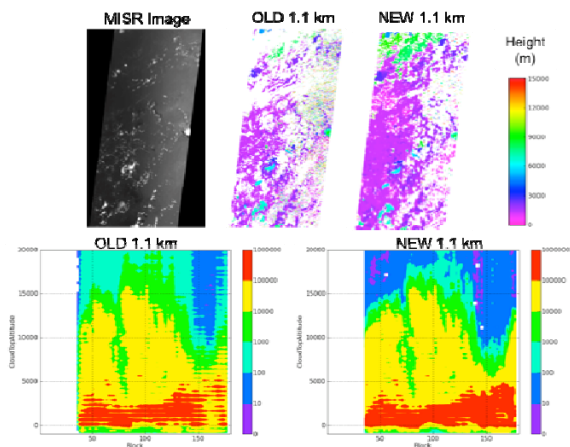

Figure 6. Improvements of the NEW over OLD algorithms in handling sun-glint contamination (top) and in reducing quantization error (bottom). The sun-glint contamination was not adequately screened by the OLD algorithm but is dealt better with the quality control of the NEW algorithm. The quantization error is a result of the fast pattern matcher at the pixel resolution. With a small overhead in computation, a sub-pixel matching helps to refine the CTH retrieval.

High-Resolution (1.1 km) CMVct and CTH Retrievals

A new product to be generated as part of the upgraded MISR algorithm, the 1.1-km cross-track CMV (CMVct), will be made available for MISR users. As shown in Figure 1, cross-track cloud motion can be determined independently from CTH, in constrast to along-track cloud motion. The cross-track disparity, a direct measurement of CMVct, can be retrieved at 1.1 km resolution with precision at or finer than the 275 m pixel resolution.

Figure 7 shows an example of simultaneous CMVct and CTH retrievals at 1.1 km resolution for the marine stratocumulus over the southeastern Pacific where the cloud sheets are filled with open and closed cells. The high-resolution retrievals reveal clearly-structured diverging/converging dynamics over the marine boundary layer. As seen in Figure 7, the cellular cloud patterns reflect inhomogeneity in CTH and CMVct, and the divergence/convergence of CMVct can be used to study shallow convection strength and lifecycle.

A good example for verifying reasonableness of the MISR 1.1-km CMVct retrieval is the convective outflow at cloud tops. Figure 8 shows an overshoot turret developed in a short period of time on the top of cloud deck of Hurricane Ida on Nov. 8, 2009. It grew so rapidly that in 7-min it expanded from a size of < 5 km to ~30 km, which is clearly evident in the consecutive views from MISR nine cameras. As shown in Figure 8, the diverging flow in the CMVct is indeed retrieved at the cloud top, showing the flows to the opposite directions outside the turret. With better CTH retrieval precision, it may be feasible to derive vertical motion from the CTH change from consecutive MISR images, and study them jointly with the divergence of CMVct in the cases like Hurricane Ida.

MISR INteractive eXplorer (MINX)

Besides the automated MISR CTH and CMV retrieval algorithm in the standard data processing, an interactive software package, called MISR INteractive eXplorer (MINX), has been developed and made available via Open Channel Foundation [*Nelson et al.*, 2008]. MINX uses the red band radiances from 7 cameras (Nadir, ±26º, ±46º, ±60º) to retrieve CMV and CTH, and has been applied to smoke and volcanic plumes. The MINX algorithm applies sub-pixel matching for every consecutive image pair in this set, and trades retrieval resolution for computationally speed. It is therefore applied in practice to a selected subset of MISR images.
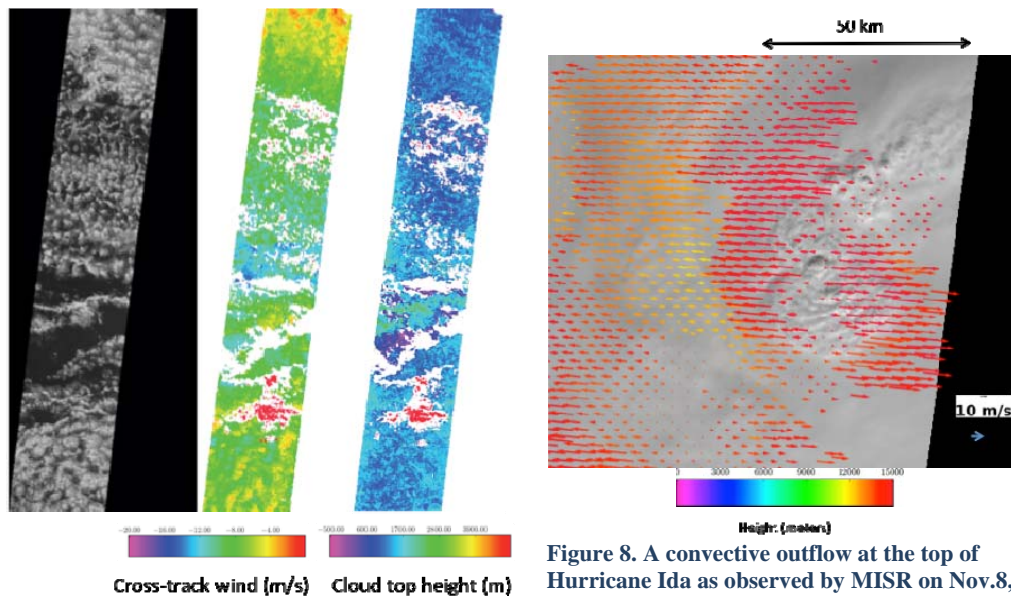

Cross-track wind (m/s)   Cloud top height (m)

Figure 7. Simultaneous high-resolution (1.1 km) CMVct and CTH retrievals from the stratocumulus over marine boundary layers.

Figure 8. A convective outflow at the top of Hurricane Ida as observed by MISR on Nov.8, 2009. The CTH and CMVct retrievals reveal a diverging overshooting turret growing from 5 km to 30 km in size within 7 min.

Similar to the standard MISR algorithm, MINX matches feature patterns (e.g., cloud, plume) from the radiance images acquired by adjacent camera pairs (e.g., Nadir-26º, 26º-46º, 46º-60º), and determines the disparity of the recognized pattern. The domain size for defining a pattern is

adjustable. In this study we use 5×5, 7×7, 9×9 pixels, respectively, for the Nadir-26º, 26º-46º, 46º-60º pairs. The disparity can be measured precisely with MINX to a sub-pixel level at the expense of intense computation, which fundamentally yields the best precision for MISR CMV and CTH retrievals. If two of six pairs produce consistent wind and height retrievals, MINX will output the results. Because cloud shapes are distorted substantially at oblique viewing angles, MINX excludes images from the ±70º viewing angles. To retrieve cloud wind vector and height, MINX requires *a priori* information about the wind direction such that cloud height and wind speed are better constrained by the disparity measurements. By specifying the wind direction, the MINX retrieval mitigates the along-track degeneracy problem without requiring large domain sizes to reduce noise.

The MINX retrieval also has some limitations. If the wind direction specified is in the along-track direction, MINX cannot retrieve the wind speed because of the full degeneracy between CTH and CMV. In addition, if the specified wind direction is wrong, the retrieval will produce incorrect CMVat coupled with a wrong CTH. In the specified polygon for digitization, or the region of interest, the MINX requires that all wind vectors must have the same direction. If a region has a complex wind field, one would need to divide the region into sub-regions such that each sub-region has the same wind direction. For good quality retrievals of MISR cloud winds, we usually apply MINX to the cases where winds are known to be primarily in the cross-track direction.

Hurricane Alberto (2000)

One of the advantages with the MISR's high-resolution CMVct and CTH retrievals is to observe the dynamical processes that are fast but occur in a small region, like the eyes of hurricanes. On 19 August 2000, MISR had an excellent view of the eye of Hurricane Alberto, providing a rare opportunity to study the inner-core dynamics and structures of the system.

Hurricane Alberto (2000) spent its entire lifetime over the open Atlantic Ocean with minimal impact on the United States. However, Alberto was an unusual storm in that it reached its peak intensity at a high latitude, north of 35˚N, after its direction was curved by a subtropical ridge. It is the seventh longest-lived storm in the Atlantic Ocean (lasting 19.75 days) with three strengthening periods in hurricane status [Figure 9], and is also one of the longest-lived Atlantic storms during August, second to Hurricane San Ciriaco (1899). It became tropical depression on 3 August and was upgraded to Tropical Storm Alberto on August 4. After a brief weakening, the storm strengthened to hurricane status on 6 August, as an eye developed in its center. Because of a vigorous upper-level low developed west of Alberto on 7-8 August, which increased vertical wind shear, it was weakened down to a tropical storm on 9 August. Starting on 10 August, Alberto strengthened and became a Category 3 hurricane again on 12 August, and curved towards the north and northeast through a break in a subtropical ridge between 11 August and 12 August. Moving east-northeastward, the hurricane began to weaken due to increasing upper-level westerlies on 13 August and 14 August and was downgraded to a tropical storm on 14 August. By then, a westerly trough that had been interacting with Alberto, causing the storm to turn abruptly to the south on 15 August, and making a large loop over the open Atlantic. On 12 August, no models forecasted this loop maneuver in the cyclone development, which would remain as a challenge of track forecasting with the current models. Alberto turned to the southwest on 16 August and to the west on 17 August. The storm then took a sharp turn toward the northwest under influence of a large, slow-moving mid-level trough off the East Coast. Alberto began to strengthen once again, and

reached hurricane status for the third time on 18 August. The hurricane continued to turn to the north on 19 August and to the northeast on 20 August and 21 August, completing the largest loop ever observed over the Atlantic Ocean.

Figure 10 shows the image of Hurricane Alberto's eye taken by MISR's nadir camera (An). Within a few hours of MISR passing overhead on 19 August 2000, the cyclone re-intensified and headed to the north. The data from the National Hurricane Center's archive suggest that the center of the cyclone moved very slowly (<2 m/s), slightly to the north, as it completed a rare loop over the Atlantic [Figure 9]. Thus, the winds in the vicinity of the eye were dominated by the rotational velocity, which can be readily derived by MINX. We first digitize the inner core dynamics of Hurricane Alberto along three cross sections (S_0, S_1, S_2) passing through the center of the eye [Figure 10]. For all the slices (S_0, S_1, S_2) across the hurricane's eyewall, we specify the wind vectors in the tangential direction with the MINX algorithm, neglecting the mean background winds. The MINX outputs include CTH, eastward and westward velocities, from which the tangential wind speed (V_θ) is derived at each CTH. The CTH and CMV retrievals are carried out at an interval of 550 m, with an estimated precision of ~1 m/s and 200 m respectively.

The cross sections (S_0, S_1, S_2) pass through Alberto's eye with different inner-core dynamics inside the eyewall. Near the eyewall, some cirrus blurs the edge and prevents MISR from seeing low clouds. Most of the low clouds inside the eyewall have an altitude <2 km. It is evident that S_0 has a mesovortex in the south end and a developing one in the north. The spans of inner-core low clouds seen by the S_0 and S_2 section are as wide as ~80 km and ~70 km, respectively, but some cirrus blocking shortens the length of S_1 view to ~60 km.
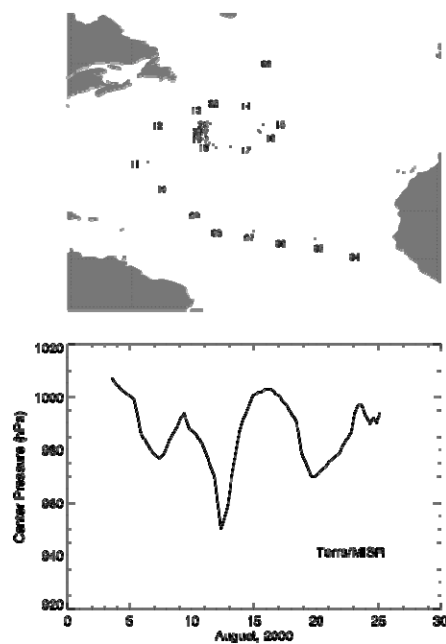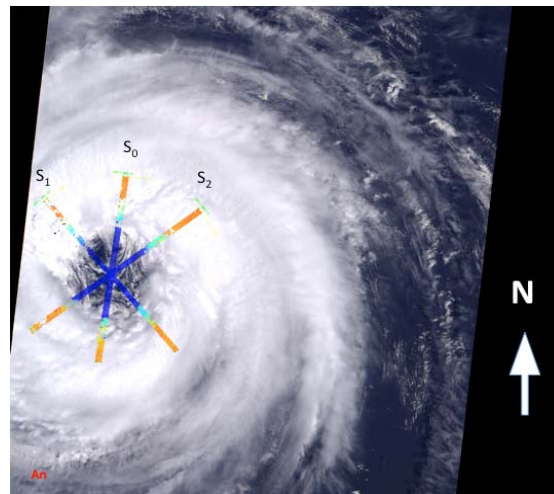

Figure 9. Hurricane Alberto's track and

Figure 10. MISR nadir (An) image of Hurricane Alberto acquired on 19 August 2000. The MINX tool is used to digitize cloud wind and height along the narrow strips (S_0, S_1, S_2) that pass through the eye center. Cloud height is colored, ranging from blue for low clouds to orange for high clouds. Under S_0, a mesovortex is clearly evident near the southern edge of

Comment [DD1]: I don't see the image

intensity during August 2000

the eyewall whereas a vortex-like feature is located in the northern edge, which was also seen in MODIS images [Kossin et al., 2002; Montgomery et al., 2002].

Figure 11 shows a slow or zero rotation near the eye center and asymmetric rotations inside the eyewall. Along the S_0 section, two distinct rotational velocities are observed in the south end where the mesovortex locates. The eye rotates at a rate ~6 time faster near the eyewall than in the center, showing ~24.8 cyc/day at $r > ~25$ km and ~4.1 cyc/day near the center. In the north end of S_0, two rotational velocities have a ratio of 2:1 but are not distinctly separated. Near the eye center, the (S_0, S_1, S_2) results all show a near-zero rotation. The S_1 section has little indication of a faster rotation near the eyewall in the either ends, but the S_2 section does. In the south end of S_2 the rotation increases gradually with the radial distance without a sharp transition, but in the north end it changes from no rotation at $r < 10$ km to 16.5 cyc/day at $r > 10$ km.

The differential rotation velocity inside the eyewall is also found in other hurricanes MISR encountered, including Hurricane Isabel on 11 Sep. 2003 and Wilma on 21 Oct. 2005. The development of faster rotation near the eyewall is thought to be associated with cyclone intensification processes (Kossin and Schubert, 2004), because the intensified jet at the eyewall enhances the barotropic instability inside the eyewall and can lead to the genesis of mesovortices. In this case, Hurricane Albedo (2000) was towards re-intensification on 19 August, reaching the peak intensity shortly after the MISR intersection.
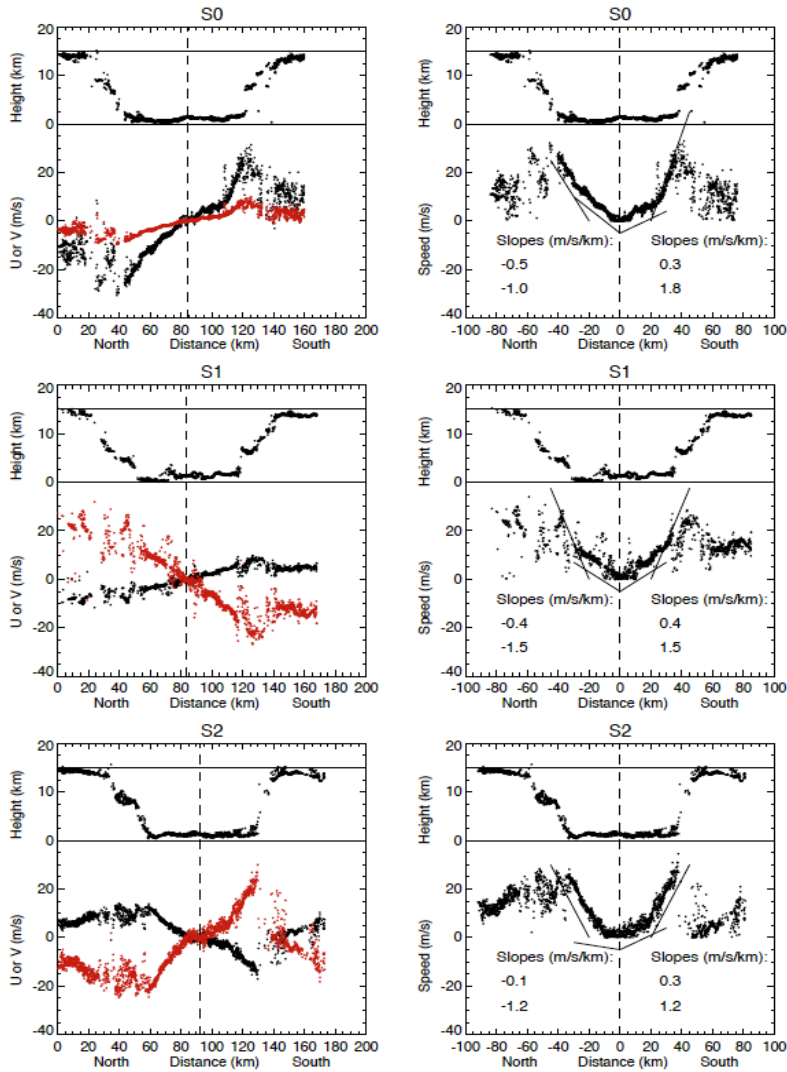
Figure 11. (Left) CTH and zonal (black) and meridional winds retrieved by MINX at 550 m resolution for the three cross sections (S₀, S₁, S₂); (right) The same CTH and the tangential wind speed (V_θ) derived from zonal and meridional winds. The slope in the figure is proportional to rotational velocity, and a factor of 13.76 can be used to convert m/s/km to cyc/day.

To examine inhomogeneity of the dynamics and structures inside the eyewall, we map the CTH and V_θ by digitizing eight sub-regions of the south and north quadrants of Alberto's eye with MINX [Figure 12]. In the south quadrant, the established mesovortex is associated with relatively lower CTHs but stronger V_θ, compared to others at the same radius. The angular inhomogeneity in

V_θ is apparently associated with the precipitation intensity underneath the eyewall. As seen in the TRMM rain rate at 15Z, which would lag the MISR by ~30 degrees due to rotation, the intensified precipitation (four centers) appear to be correlated with MISR cloud clusters and fast V_θ retrievals.
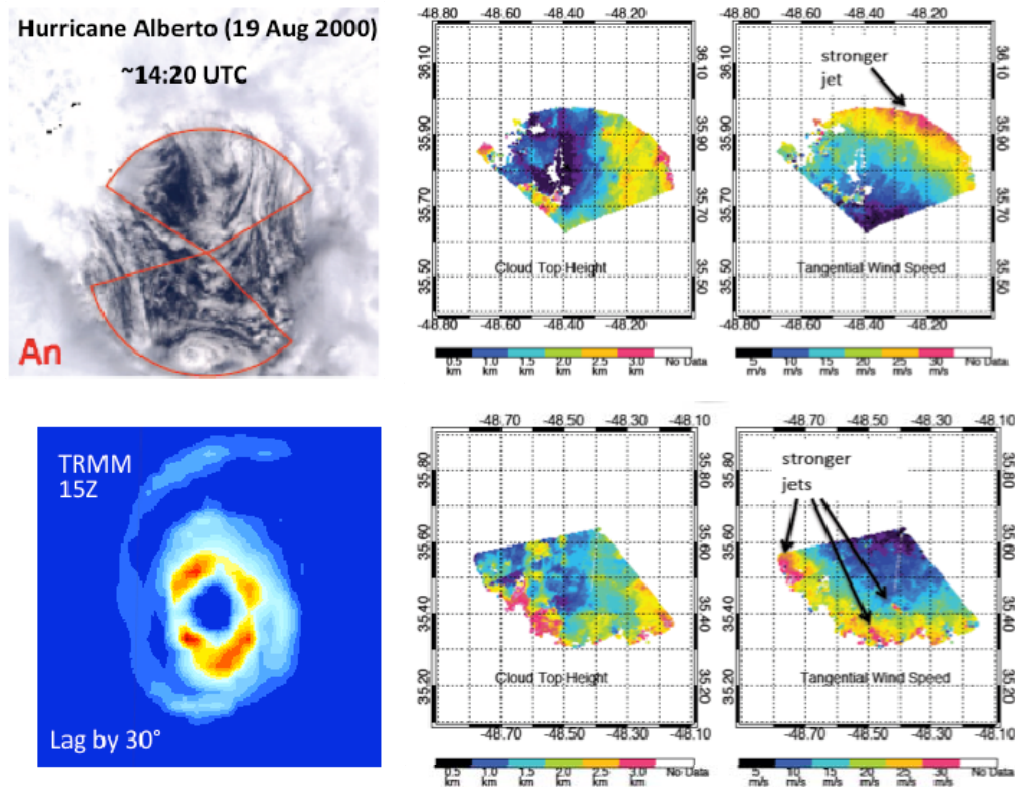

Figure 12. Distributions of Alberto's inner core CTH and V_θ. The CTH and V_θ maps inside Alberto's eye. The MINX analysis regions are indicated on the An camera, with foci on the southern and northern parts of the eye where V_θ are mostly in the MISR cross-track direction and the quality of the retrieved winds is best. In each of the regional analysis, there are eight sub-regions (or slices of a pie) for which the MINX tool is applied separately with the specified tangential wind direction. The retrieved cloud heights and V_θ from the sub-regions are displayed together as a map for the southern (bottom) and northern (top) parts of the eye. Data with cloud top height greater than 3 km are not shown.

Despite danger to flight crews, numerous airborne observations have been taken to better understand dynamics and structures of precipitation and clouds inside the eye of tropical cyclones. Black and Willoughby (1992) studied Hurricane Gilbert (1988) for eyewall replacement, and found that the outer eyewall strengthened and contracted while the inner eyewall weakened and was eventually replaced. Marks et al. (2008) reported a more detailed view of the inner-core dynamics and structure of Hurricane Hugo using aircraft data acquired at 450 m altitude on 15 September 1989. By penetrating deep into the intense cyclonic vorticity, they obtained

measurements near the strongest convection in the eyewall for eyewall vorticity maximum (EVM). They found that V_θ decreases linearly but sharply inward from the radius of maximum wind (i.e., $V_\theta = V_{\theta\,max}$ at $r = r_{max}$). The steepest gradient of V_θ occurred at $r = \sim 7$ km with V_θ changing from ~70 m/s to ~20 m/s within ~0.5 km. For $r < 6.5$ km, the rotational velocity became significantly weaker to ~3 m/s/km.
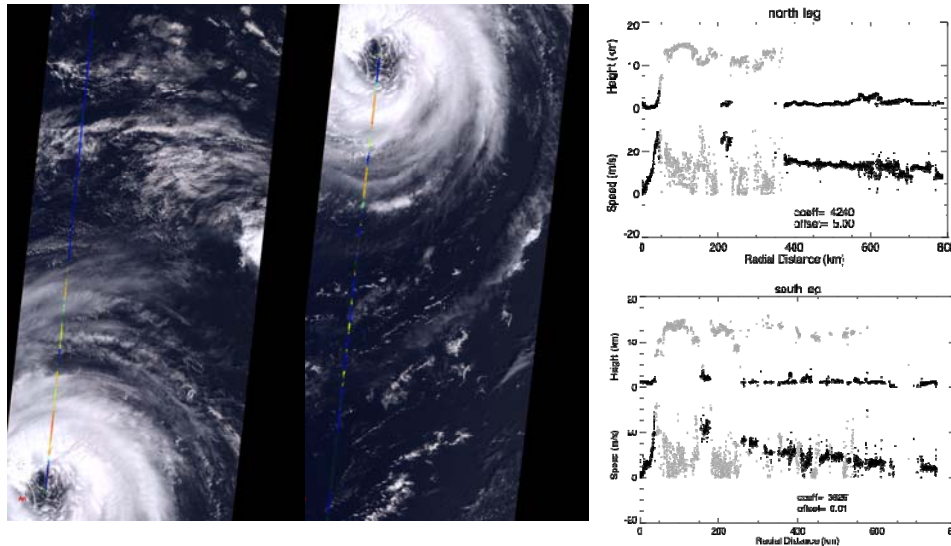

Figure 13. Outer-core dynamics from a south and north leg of the MISR swath. Outside the eyewall, MISR observes some boundary-layer clouds through the gaps between high clouds. The tangential wind speeds over ~800 km are retrieved as a function of the radius from the center for the north and south leg. The wind speeds at heights < 4 km are fitted to $V_\theta = M/r + V_0$, where M is approximately the absolute angular momentum and V_0 is the background wind.

The sharp breaking point in the aircraft observations bears great similarity to the MISR observations in Figure 11. Outward from r_{max} to 40 km, V_θ decreased exponentially and fitted well to a power law (e.g., Mallen et al., 2005): $V_\theta = V_{\theta\,max}\,(r_{max}/r)^\alpha$, where $\alpha = 0.83$. For the Hurricane Alberto case, we also find that the power law with $\alpha = 1$ fits well to the MISR boundary-layer CMVs up to 800 km in radius (Figure 13). For a south and north leg of the MISR swath, we obtained $V_\theta = 3825/r$ and $V_\theta = 4240/r + 5$, respectively, where V_θ is in m/s and r in km. The north leg winds approach to a 5 m/s background wind (mostly easterly) whereas the south leg shows no significant background wind.

TC Intensity and Inner-Core Rotation

Observations have played a critical role in improving our understanding and prediction of tropical cyclones (TCs) over the last 50 years. Most of the TC lifetime is spent over ocean, where detailed atmospheric observations of inner-core cyclone dynamics and structures are limited. As a

result, model initialization and parameterization are poorly constrained when they are needed for predicting cyclone intensity.

MISR high-resolution retrievals of V_θ inside TC eyewalls allow us to examine the relationship between inner-core rotation and cyclone intensity more quantitatively. Since many of the Atlantic hurricanes were well documented, observed, and analyzed, we focus on these cases and compare them with MISR V_θ retrievals. Among the cases analyzed, we find that the inner-core rotation is often characterized by a strong gradient in rotational velocity, some of which have a distinguishable break point. As illustrated in Figure 14, the core rotates faster near the eyewall, which appears to be associated with the center pressure. For the five Atlantic hurricanes studied (Figure 15), we find a good relation between near-eyewall V_θ and the hurricane center pressure. Because of the asymmetry of cyclone rotation, in each case we estimated the near-eyewall rotation from the north and south segment of the eye where MISR has the best sensitivity to V_θ. As shown in Figure 15, the hurricane center pressure appears to relate linearly with the estimated rotational velocities. If the fast rotation near the eyewall is proportional to cyclone intensity, the high-resolution stereo technique like MISR could be used for measuring hurricane intensity.
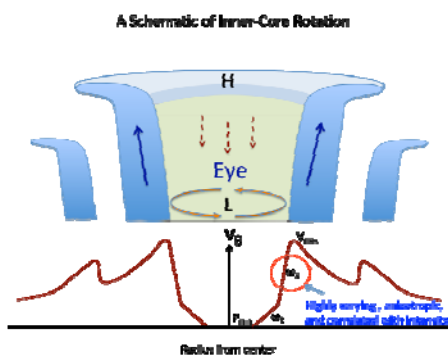

Figure 14. A schematic view of TC inner-core rotation, showing a faster rate near the eyewall and a slower or little rotation at the center. The faster rotation is found to relate linearly with cyclone intensity.
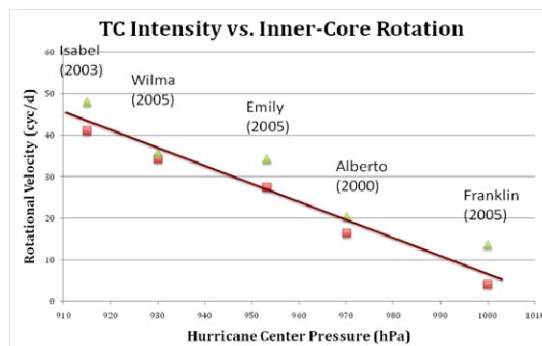
Figure 15. Relationship between MISR-observed rotation velocities and the cycle center pressures from the best track analysis for five Atlantic hurricane cases. The symbols are the estimates based on the southern and northern segments of the inner core.

Concepts for Future Weather and TC Observations

For the stereo techniques based on pattern matching, the requirement for radiometric calibration is not as stringent as for aerosol measurements with MISR. Therefore, the system can be greatly simplified for much less power and mass. A compact instrument concept, namely WindCam, proposed by Diner et al. (2008), can provide 7 viewing angles from a single lens at the red-band wavelength, which has only 17 kg in mass and 23 W in power, compared to 150 kg and 75 W for MISR (Figure 16). Such a light, low-power instrument makes it easy to access space and flexible to board on various platforms, particularly, small satellites in LEO (Low Earth Orbit) or

MEO (Medium Earth Orbit). For example, two identical multiangle systems can be flown in tandem to each other to produce precise wind speeds in both cross- and along-track directions. As discussed above, multiangle cameras from a single platform produce noisier wind measurements in the along-track direction than in the cross track, due to degeneracy between the parallax from cloud height and the along-track cloud motion. A dual-satellite system will mitigate such a problem with simultaneous views from two different angles and yield unambiguous retrievals of CTH and CMVat.

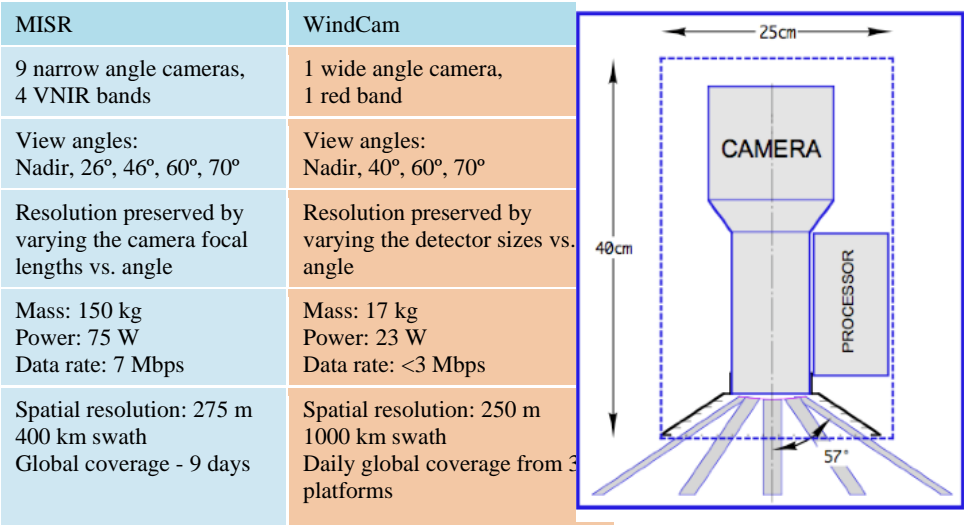| MISR	WindCam	
9 narrow angle cameras, 4 VNIR bands	1 wide angle camera, 1 red band	
View angles: Nadir, 26°, 46°, 60°, 70°	View angles: Nadir, 40°, 60°, 70°	
Resolution preserved by varying the camera focal lengths vs. angle	Resolution preserved by varying the detector sizes vs. angle	
Mass: 150 kg Power: 75 W Data rate: 7 Mbps	Mass: 17 kg Power: 23 W Data rate: <3 Mbps	
Spatial resolution: 275 m 400 km swath Global coverage - 9 days	Spatial resolution: 250 m 1000 km swath Daily global coverage from 3 platforms	

Figure 16. MISR vs. WindCam concept. Relaxed radiometric calibration enables a light and power-efficient instrument like WindCam to fly on small satellites.

Like MISR, the WindCam concept is a pushbroom imager without moving parts, which can be operated together with other instruments such as GPS radio occultation (RO) and GRACE (Gravity Recovery And Climate Experiment) that require a stable platform. GPS RO on small satellites, like COSMIC (Constellation Observing System for Meteorology, Ionospheric, and Climate), has made a great impact on data assimilation in numerical weather prediction (NWP). Together, synergy among WindCam, GPS RO, and GRACE science can yield high returns for weather and climate research from future small satellite missions.

References:

Black, M. L., and H. E. Willoughby, The concentric eyewall cycle of Hurricane Gilbert. Mon. Wea. Rev., 120, 947-957, 1992.

Davies, R., Á. Horváth, C. Moroney, B. Zhang, and Y. Zhu, Cloud motion vectors from MISR using sub-pixel enhancements, *Remote Sens. Environ.,* **107**, 194–199, 2007.

Diner, D. J., et al., The value of multiangle measurements for retrieving structurally and radiatively consistent properties of clouds, aerosols, and surfaces. *Remote Sensing of Environment* **97**, 495 – 518, 2005.

Diner, D. J., et al., WindCam and MSPI: Two cloud and aerosol instrument concepts derived from Terra/MISR heritage. Proceedings of SPIE, the International Society for Optical Engineering   ISSN 0277-786X, vol. 7081, pp. 70810T.1-70810T.9, 2008.

Garay, M. J., S. P. de Szoeke, and C. M. Moroney, Comparison of marine stratocumulus cloud top heights in the southeastern Pacific retrieved from satellites with coincident ship-based observations, *J. Geophys. Res.*, **113**, D18204, doi:10.1029/2008JD009975, 2008.

Hinkelman, L. M., R. T. Marchand, and T. P. Ackerman, Evaluation of MISR cloud motion vectors using NOAA radar wind profiler data, *J. Geophys. Res.*, 114, Article Number: D21207, doi:10.1029/2008JD011107, 2009.

Holz, R. E., et al., Global Moderate Resolution Imaging Spectroradiometer (MODIS) cloud detection and height evaluation using CALIOP, *J. Geophys. Res.*, **113**, D00A19, doi:10.1029/2008JD009837, 2008.

Horváth, Á., and R. Davies, Simultaneous retrieval of cloud motion and height from polar-orbiter multiangle measurements, *Geophys. Res. Lett.*, **28**, 2915–2918, doi:10.1029/2001GL012951, 2001.

Jovanovic, V., B. Ledeboer, M. Smyth, and J. Zong (2001). Georectification of the Airborne Multi-angle Imaging SpectroRadiometer. ISPRS joint workshop, "High Resolution Mapping From Space 2001".

Kossin, J. P., B. D. MCNOLDY, AND W. H. SCHUBERT, Vortical Swirls in Hurricane Eye Clouds, Mon. Wea. Rev., 130, 3144-3149, 2002.

Kossin, J. P., and W. H. Schubert, Mesovortices in hurricane Isabel. BAMS, 151-153, February, 2004.

Marchand, R. T., T. P. Ackerman, and C. Moroney, An assessment of Multiangle Imaging Spectroradiometer (MISR) stereo-derived cloud top heights and cloud top winds using ground-based radar, lidar, and microwave radiometers, *J. Geophys. Res.*, **112**, D06204, doi:10.1029/2006JD007091, 2007.

Marks, F. D., et al., Structure of the eye and eyewall of Hurricane Hugo (1989). Mon. Wea. Rev., 136, 1237-1259, 2008.

Montgomery, M. T., V. A. Vladimirov, and P. V. Denissenko: An experimental study on hurricane mesovortices. *J. Fluid Mech.,* **471,** 1–32, 2002.

Moroney, C., R. Davies, and J.-P. Muller, Operational retrieval of cloud-top heights using MISR data, *IEEE Trans. Geosci. Remote Sens.*, **40**, 1532–1540, doi:10.1109/TGRS.2002.801150, 2002.

Mueller, K.J., L. Di Girolamo, M. Fromm, S. Palm, Stereoscopic detection and analysis of polar stratospheric clouds, Geophys. Res. Lett., 35, L17183, 2008.

Muller, J.-P., A. Mandanayake, C. Moroney, R. Davies, D. J. Diner, and S. Paradise, MISR stereoscopic image matchers: Techniques and results, *IEEE Trans. Geosci. Remote Sens.*, **40**, 1547–1559, doi:10.1109/TGRS.2002.801160, 2002.

Nelson, D. L., Y. Chen, R. A. Kahn, D. J. Diner, and D. Mazzoni, Example applications of the MISR INteractive eXplorer (MINX) software tool to wildfire smoke plume analyses, *Proc. of SPIE, 7089*, 708909, doi:10.1117/12.795087, 2008.

Zong, J., R. Davies, J.P. Muller, and D.J. Diner (2002). Photogrametric retrieval of cloud advection and top height from the multi-angle imaging spectroradiometer (MISR). *Journal of the American Society for Photogrammetric Engineering and Remote Sensing*, **68** (8), 821-830.